Science of the Total Environment 571 (2016) 380–387

Contents lists available at ScienceDirect

Science of the Total Environment

journal homepage: www.elsevier.com/locate/scitotenv

Cu/Cu_2O/CuO loaded on the carbon layer derived from novel precursors with amazing catalytic performance

Xiaoli Zhao [a], Yixin Tan [a,b], Fengchang Wu [a,*], Hongyun Niu [b], Zhi Tang [a], Yaqi Cai [b], John P. Giesy [a,c]

[a] State Key Laboratory of Environmental Criteria and Risk Assessment, Chinese Research Academy of Environmental Sciences, Beijing 100012, China
[b] State Key Laboratory of Environmental Chemistry and Ecotoxicology, Research Center for Eco-Environmental Sciences, Chinese Academy of Sciences, Beijing 100085, China
[c] Department of Veterinary Biomedical Sciences and Toxicology Centre, University of Saskatchewan, Saskatoon, Saskatchewan, Canada

HIGHLIGHTS

- We present an effective catalyst for reductive degradation of organic dyes and phenols in water.
- Compared with noble metals, Cu/Cu_2O/CuO@C particles are more efficient and less expensive
- The porous structure provided a large contact area and channels for the pollutions and active site.

GRAPHICAL ABSTRACT

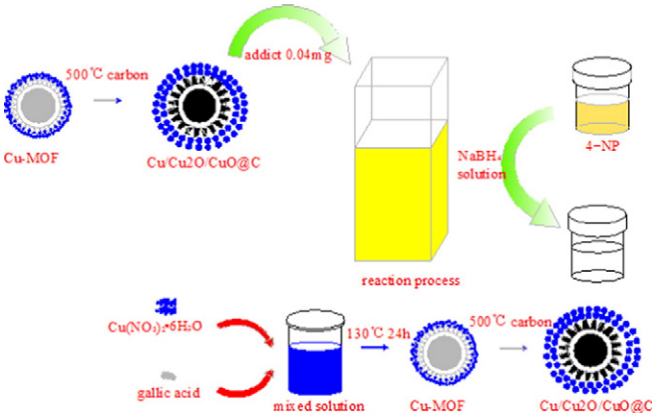

ARTICLE INFO

Article history:
Received 24 March 2016
Received in revised form 20 May 2016
Accepted 20 May 2016
Available online 21 July 2016

Editor: J Jay Gan

Keywords:
Cu/Cu2O/CuO@C
Synthesis
Catalyst
Organic dyes
Phenols

ABSTRACT

A simple, novel method for synthesis of Cu/Cu_2O/CuO on surfaces of carbon (Cu/Cu_2O/CuO@C) as a non-noble-metal catalyst for reduction of organic compounds is presented. Compared with noble metals, Cu/Cu_2O/CuO@C particles are more efficient and less expensive. Characterization of the Cu/Cu_2O/CuO@C composites by high-resolution transmission electron microscope (HRTEM), x-ray diffraction (XRD), infrared spectroscopy and Raman analysis, revealed that it was composed of graphitized carbon with numerous nanoparticles (100 nm in diameter) of Cu/CuO/Cu_2O that were uniformly distributed on internal and external surfaces of the carbon support. Gallic acid (GA) has been used as both organic ligand and carbon precursor with metal organic frameworks (MOFs) as the sacrificial template and metal oxide precursor in this green synthesis. The material combined the advantages of MOFs and Cu-containing materials, the porous structure provided a large contact area and channels for the pollutions, which results in more rapid catalytic degradation of pollutants and leads to greater efficiency of catalysis. The material gave excellent catalytic performance for organic dyes and phenols. In this study, Cu/Cu_2O/CuO@C was used as catalytic to reduce 4-NP, which has been usually adopted as a model reaction to check the catalytic ability. Catalytic experiment results show that 4-NP was degraded approximately 3 min by use of 0.04 mg of catalyst and the conversion of pollutants can reach more than 99%. The catalyst exhibited little change in efficacy after being utilized five times. Rates of degradation of dyes, such as Methylene blue (MB) and

* Corresponding author.
E-mail addresses: zhaoxiaoli_zxl@126.com (X. Zhao), wu_fengchang@126.com (F. Wu).

http://dx.doi.org/10.1016/j.scitotenv.2016.05.151
0048-9697/

Rhodamine B (RhB) and phenolic compounds such as O-Nitrophenol (O-NP) and 2-Nitroaniline (2-NA) were all similar.

1. Introduction

Metal-Organic Frameworks (MOFs) with ordered networks, well-defined pores and large surface area have been widely used in many fields such as sensing, drug delivery, gas adsorption and so on (Kreno et al., 2012; Patricia et al., 2010; Schlichte et al., 2004; Zhao et al., 2015). In general, MOFs are utilized as Lewis acid catalysts due to their acidic metal center (Dhakshinamoorthy and Garcia, 2012; Mitchell, 2013), high surface area and tunable porosity. But the weak stability of MOFs in water limits their utility in aqueous systems. Therefore, researchers have paid attention to synthesis various kinds of MOFs to optimize their performance. Metal nanometer materials are unstable and tend to self-aggregation due to their super surface energy, which might influence their application, efficiency and potential to be recycled (Niu et al., 2016). To solve this problem, excellent highly porous, supporting matrices to provide accessible channels for target organic molecules to contact metal nanoparticles are needed. Noble metals such as gold (Au), silver (Ag) and platinum (Pt) have been used to as catalysts (Zhu et al., 2013; Leung et al., 2012), but their expensiveness and scarcity limit their application and scope. Therefore, to degrade organic contaminants in water, it was considered urgent to develop non-noble metal materials with effective catalytic properties that were also stable in water.

Attention has been focused on Cu-containing materials. Cu-MOF has a greater capacity to adsorb higher hydrogen than does Zn-MOF (Panella et al., 2006). When Cu-MOF was used as the catalyst for "Click" reactions, it was found that different organic linkers in the MOF influenced catalysts. Based on this information a one-pot, two-step process was developed to remove phenylacetylene from water (Luz et al., 2010). However, stability of MOF in water is not good so other forms of metal oxide and MOF have been studied. When Cu@Cu_2O was synthesized as core–shell microspheres to explore photocatalytic activity, it exhibited greater photo-catalytic decomposition of gaseous nitrogen monoxide under visible light irradiation than did simple Cu_2O (Ai et al., 2009).

Preparation of rare Cu products used in removing dyes and phenols from water can be time consuming and complicated. Therefore, here a novel, simple and efficient scheme (Fig.1) to fabricate Cu-MOF by Cu metal and gallic acid (GA) is presented. GA has been used in the green synthesis of AgNPs and AuNPs as well (Yoosaf et al., 2007). However, to the best of our knowledge, GA has not been utilized as organic ligands to synthesize hierarchical structured nanoparticles.

In this study, GA was used as both organic ligand and carbon precursor with MOF as the sacrificial template and metal oxide precursor. Cu/Cu_2O/CuO which has excellent catalytic performance was loaded onto the carbon layer which had been carbonized under nitrogen. Cu/Cu_2O/CuO@C not only has the advantage of porosity with large specific surface area, but also possesses catalytic performance as good as those of noble materials. Besides, different pore sizes of Cu/Cu_2O/CuO distributed on inner and outer surface of carbon, which provided channels for target organic molecules to access active catalytic sites. The material can be reused so as to reduce effects on the environment. Capabilities of the novel catalytic materials were used for reductive degradation of dyes and phenols in water.

2. Materials and methods

2.1. Chemicals and materials

Copper (II) nitrate hydrate, ethanol (C_2H_5OH, 99.7%), and N, N-Dimethylformamide (DMF, 99.5%) were purchased from Sinopharm Chemistry Reagent Co., Ltd. (Beijing, China). Gallic acid and 4-Nitrophenol(4-NP), Methylene blue(MB), Rhodamine B(RhB), *O*-Nitrophenol (*O*-NP), 2-Nitroaniline(2-NA) were obtained from J&K Chemical Ltd. (Beijing, China). Ultrapure water used in all of the experiments was prepared by use of a Milli-Q SP reagent water system (Millipore, Bedford, MA, USA).

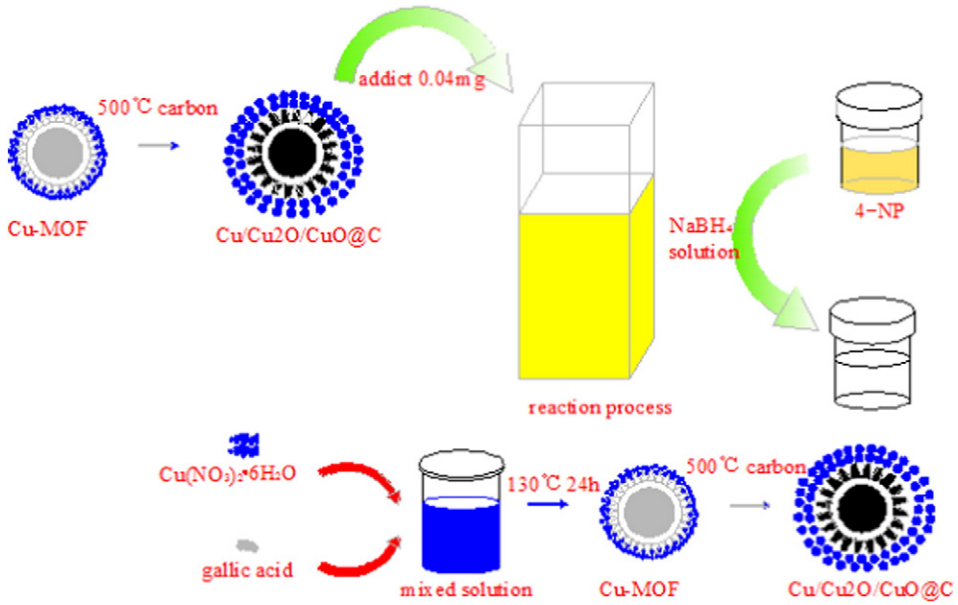

Fig. 1. Catalytic reaction process of 4-NP and schematic diagram of the Cu/Cu_2O/CuO@C synthetic strategy.

2.2. Synthesis of Cu-GA

An aliquot of 0.9664 g copper (II) nitrate hydrate along with 0.7526 g gallic acid were put in a 100 mL, Teflon-lined, stainless-steel autoclave, adding 40 mL Dimethyl formamide (DMF) with stirring or ultrasound to dissolve the solid (ultrasonic cleaner, KQ-500DE, 500 W, 40 kHz). After completely dissolving, sealed to heat at 130 °C for 24 h and washed with DMF and ethanol three times after reaction and air cooled to room temperature to purify the product, then centrifuged and dried at 50 °C under vacuum environment for 24 h.

2.3. Synthesis of $Cu/Cu_2O/CuO@C$

The product of the reaction was ground in a mortar and pestle then removed to a quartz tube to be carbonized under nitrogen at 500 °C for 4 h. The material was cooled to room temperature and ground again before use.

2.4. Characterization of material

Morphological characteristics were determined by transmission electron microscope (TEM, model H-7500 Hitachi, Japan) and a scanning electron microscopy-energy dispersive X-ray spectrometry (SEM, EDS model Hitachi S-2400, Tokyo, Japan). Crystallographic information of the material was determined by use of powder, X-ray diffraction (XRD, Almelo, Netherlands) which used a Cu Ka radiation ranging from 5 to 90 with a resolution of 0.02. Quantification of surface area, pore size and volume were accomplished by use of BET methods (ASAP2000 V3.01A; Micromeritics, Norcross, GA). FTIR spectra were recorded on a NEXUS 670 Infrared Fourier Transform Spectrometer (Nicolet Thermo, Waltham, MA) after pelletizing with KBr in the range of 4000–400 cm^{-1}. TGA (Q500 V3.15) were heated at a rate of 10 °C/min up to 900. Surface characteristics were also investigated by use of X-ray photoelectron spectroscopy (XPS with a monochromatic Al Kα X-ray source).

2.5. Catalytic reduction of 4-NP

Catalytic experiments were conducted in reaction vessel to which 2 mL deionized water, 1 mL $NaBH_4$ (0.2 M), 0.1 mL 4-NP (5 mM) and 50 uL catalyst solution (2 mg mL^{-1}) were added. Reaction was conducted under room temperature without stirring while the whole process, no adjusting of pH was needed. The concentration was measured every 40 s without reaction stopping. Color of the solution gradually vanished as the reaction proceeding and was completely gone within 3 min. Progress of reactions were followed by use of ultraviolet–visible (UV–vis) spectrometry at specific time intervals. After reduction was complete, catalyst was separated by centrifuge and then reused in the next cycle. The catalytic reduction of other nitrobenzenes was conducted under the same conditions as those specified for 4-NP.

3. Results and discussions

3.1. Characterization and properties of adsorbents

Transmission electron microscopy (TEM) images have shown that Cu-GA and $Cu/Cu_2O/Cu@C$ particles were shaped like chrysanthemum with the size of Cu particles of approximately 100 nm attached to edges of the petals (Fig. 2A and Fig. 2B). SEM images of Cu-GA and $Cu/Cu_2O/Cu@C$ are shown (Fig 2C and Fig.2D). HRTEM images of $Cu/Cu_2O/Cu@C$ (Fig. 2E and Fig. 2F) indicated that this material has a crystalline structure. After carbonization, some particles had rough rims with a chrysanthemum-like shape.

Crystal phases of the samples are investigated by XRD analysis (Fig.3A). The XRD pattern of Cu-GA is totally different from that of $Cu/Cu_2O/CuO@C$ and GA powder. Peaks occurring at 10.26°, 41.79°, 43.27°, 50.39°, suggest the chelation of Cu atoms and GA in Cu-GA. In the XRD pattern of $Cu/Cu_2O/CuO@C$, the distinguishing characteristic peaks appear at $2\theta = 29.5°, 34.5°, 42.2°, 61.5°, 67.9°, 73.4°$ which can be attributed to the (110), (111), (200), (220), (310) and (311) diffraction planes of Cu_2O (JCPDS#5-667). Peaks appearing at 32.5° (110), 36.4° (111), 38.6° (200), 48.7° (20-2), 53.4° (020), 58.2° (202), 66.1° (31-1), 51.3° (200) and 72.3° (220) are representative of the Cu. The strong, sharp peaks indicate the crystalline nature of the sample. The height and amount of the characteristic diffraction peaks can be used for calculating the contents of various forms of copper. The greatest proportion of Cu occurs as Cu_2O, followed by CuO and Cu.

The FTIR spectrum (Fig. 3B) was used to detect molecules on surfaces of the material. By comparing spectra of GA and Cu-GA, the broad peak at 3329 cm^{-1}, which corresponds to phenolic groups in gallic acid and is due to the stretching vibration of O—H, becomes narrow and small. Bands centered at 1600 cm^{-1} and 1366 cm^{-1} result from the stretch of COO– in the benzene of GA (Bai et al., 2008; Bai et al., 2010; Zhou et al., 2013). After interaction with Cu, the O—H stretching band at 3429 cm^{-1}, Cu—O bending peaks at 493 cm^{-1}, and bending band of O—H in carboxylic groups at 1029 cm^{-1} disappear, which indicates

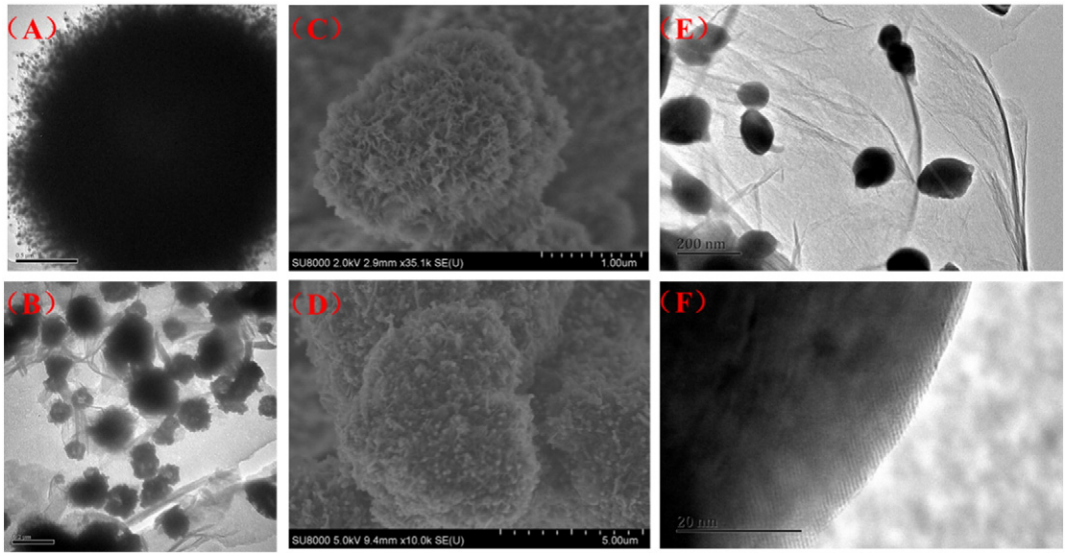

Fig. 2. TEM images of Cu-GA(A), $Cu/Cu_2O/CuO@C$(B), SEM images of Cu-GA(C) and $Cu/Cu_2O/CuO@C$(D), HRTEM image of $Cu/Cu_2O/CuO@C$ (E, F).

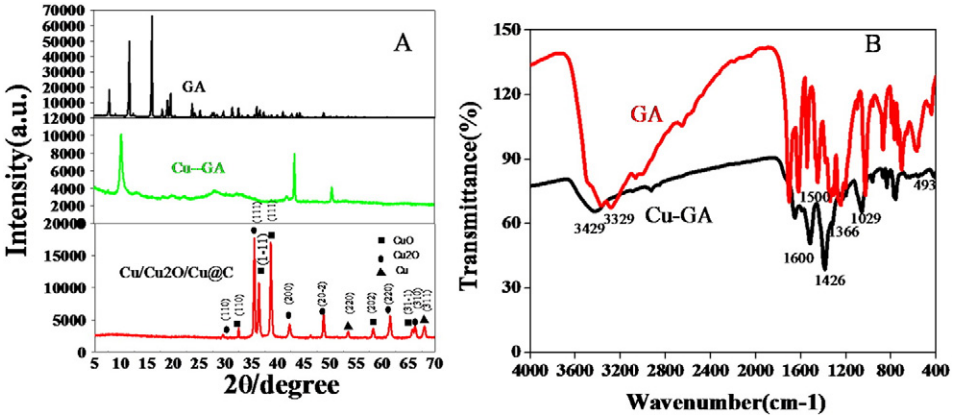

Fig 3. XRD spectra of Cu-GA and Cu/Cu_2O/Cu@C from 2θ = 5 to 90°, FTIR spectra of GA, Cu-GA (B).

that all phenolic and carboxylic groups in GA were chelating Cu (Zhou et al., 2013). Correspondingly, the stretching bend of C═O in the spectrum of Cu-GA shifted to a lesser frequency, and two characteristic bands of the carboxylate groups (COO–) between 1300 and 1600 cm^{-1} appeared. Asymmetrical stretching occurred at 1500 cm^{-1} with stretching at 1426 cm^{-1}. These results indicated that all carboxylic and phenolic groups were interacting with Cu. Carboxylic groups are vital for formation of the chrysanthemum-like structure of the materials. The hierarchical morphology of the products would not be observed if tannic acid had been used as the linker. In the spectrum of Cu/Cu_2O/CuO@C, peaks characteristic of carboxylic groups, phenolic groups and benzene rings generally disappeared, which suggested successful carbonization of GA; the broad peaks in the region of 3600–3300 cm^{-1}, and 1670–1550 cm^{-1} correspond to the surface-sorbed water and hydroxyl groups of carbon materials.

XPS (Fig. 4C) was used to investigate chemical composition and oxidation state of the surface of Cu/Cu_2O/CuO@C. The spectrum (Fig. 4C) shows that the material contained the elements Cu, O and C. The $Cu^{2p3/2}$ spectrum contained two peaks at 932.1 and 933.8 eV, respectively. The peak at 932.1 eV was assigned to Cu_2O/Cu (Cu^+/Cu^0). The similar binding energies of Cu^+ and Cu^0 make it difficult to distinguish Cu_2O (Cu^+) from Cu^0 by XPS, but this result is consistent with other reports (Ghodselahi et al., 2008; Du et al., 2003; Jia et al., 2009). The coexistence of Cu and Cu_2O in the synthesized material was also confirmed by use of XRD. The peak at 933.8 eV is due to CuO, although it is slightly higher than the reported energy of CuO (933.7 eV) (Wagner et al., 1979), it agrees well with other values reported for CuO surface phase (Wagner et al., 1979; Espinós et al., 2002; Zhu et al., 2004; Wang et al., 2003 Wang et al., 2002; Xu et al., 1999; Hui et al., 2002; Brookshier et al., 1999; Fernando et al., 2002). The, three peaks of 530.2, 531.6, 533.6 eV observed in the O1s spectrum (Fig. 4C) are consistent with the broad peak of O1s, the peak at 530.2 eV is consistent with O1s of Cu_2O that have been reported previously, which are in the range of 530.0–530.7 eV (Wagner et al., 1979; Espinós et al., 2002; Zhu et al., 2004; Wang et al., 2003; Wang et al., 2002). O1s in CuO appears at 533.6 eV and the peak at 531.6 eV was assigned to other oxygen

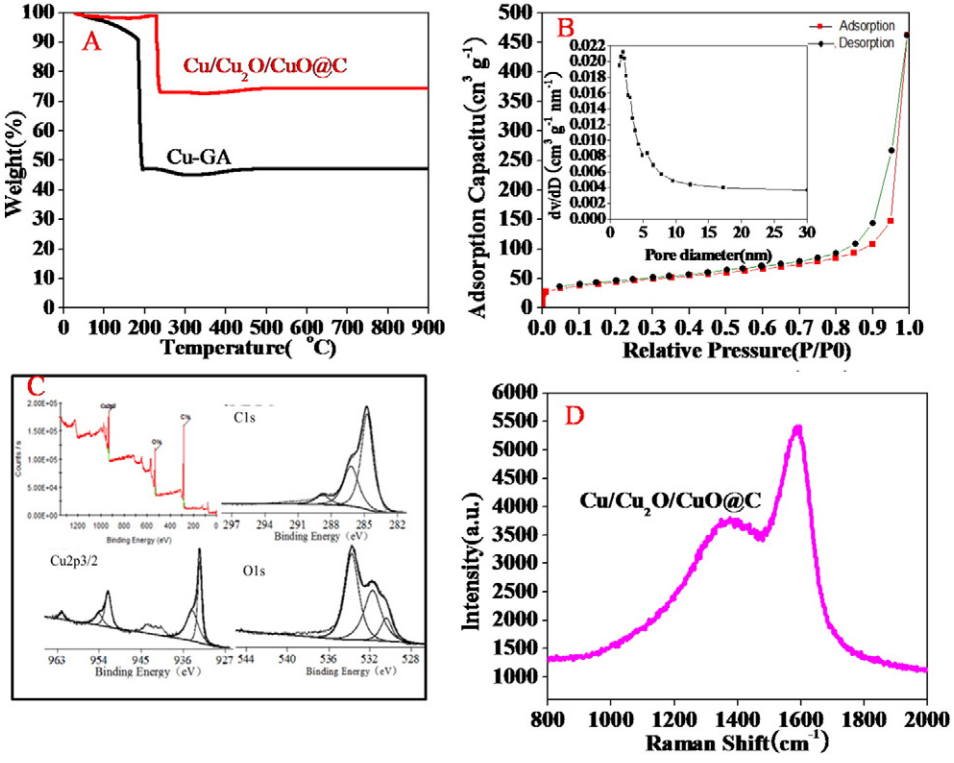

Fig. 4. TGA curves (A), N_2 adsorption/desorption isotherm (B), fitted XPS spectra of C1s, Cu2p3/2, O1s (C) and Raman spectra (D) of Cu/Cu_2O/Cu@C.

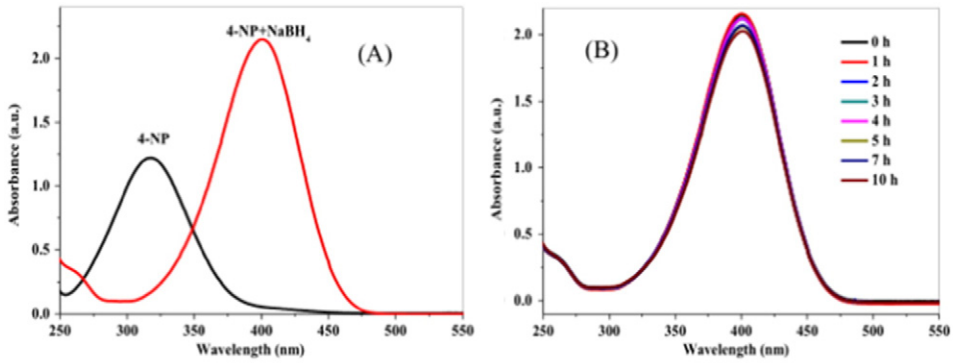

Fig. 5. UV–vis absorption spectra of the solution of 4-NP with and without $NaBH_4$ (A), time-dependent UV–vis absorption spectra of the 4-NP reduced by $NaBH_4$ without catalyst (B).

components such as OH, H_2O and species of carbonate on the surface. The C1s core levels for Cu-GA present three main components related to C-OH, COO– and C—C species (Fig.4C). The corresponding binding energy appeared at 286.2 eV, 289 eV and 284.7 eV, respectively. The peaks observed in the XPS spectrum are conclusive evidence of the existence of $Cu/Cu_2O/CuO@C$.

The thermal gravity analysis (TGA) curve of Cu-GA exhibited a slight decrease at about 150 °C, which can be attributed to loss of water on the surface, then a sharp drop at about 200 °C due to the decomposition of Cu-GA. From these observations it can be concluded that the carbon and other residues content was 42%. The TGA curve of $Cu/Cu_2O/CuO@C$ (Fig. 4A) shows that the carbon phase in $Cu/Cu_2O/CuO@C$ decomposes promptly suggesting oxidation of carbon. The percent remaining can be attributed to the mixture of $Cu/Cu_2O/CuO$. Rapid loss of mass in the range of 200–250 °C, is likely due to decomposition of the precursor into Cu_2O/CuO and CO_2 (Fig. 4A). The mass percentage of $Cu/Cu_2O/CuO$ particles and carbon was calculated to be 70%. In the Raman spectrum of $Cu/Cu_2O/CuO@C$ (Fig. 4D), two peaks centered at 1588 cm^{-1} which represents the G-line and 1375 cm^{-1} representing the D-line can be attributed to in-plane vibrations of crystalline graphite and disordered amorphous carbon, respectively. This observation suggests that GA linkers had been successfully graphitized. Together, the above-mentioned results imply that $Cu/Cu_2O/CuO@C$ was composed of $Cu/Cu_2O/CuO$ and graphitized carbon. From the data gathered for characterization of particles, which are derivatives of Cu on carbon, it can be inferred that the particles are $Cu/Cu_2O/CuO@C$.

The N_2 adsorption/desorption isotherm and calculated pore size distribution of $Cu/Cu_2O/CuO@C$ (Fig. 4B) suggest that the process of adsorption is the IV-type with H3-type hysteresis loops. The pore size of 3.85 nm is classified as mesoporous. The total pore volume of $Cu/Cu_2O/CuO@C$ was determined by use of the Barrett–Joyner–Halenda (BJH) adsorption method to be 0.704 $cm^3\ g^{-1}$. The average pore size calculated from the desorption branch of the N_2 isotherm by the BJH method was 3.85 nm which corresponds to the isotherm of typical mesoporous materials and the Brunauer–Emmett–Teller (BET) surface area of the obtained $Cu/Cu_2O/CuO$ composite was 154.6 $m^2\ g^{-1}$.

3.2. Catalytic capability

Cu_2O solids and mono-crystals have been used as photo-catalysts for removal of organic pollutants by degradation under visible light (SU et al., 2011). The reaction $NaBH_4$ catalytic reduction of removing 4-nonylphenol (4-NP) has been adopted as a model reaction to check the catalytic ability of metal NPs, the daughter derivatives may be 4-

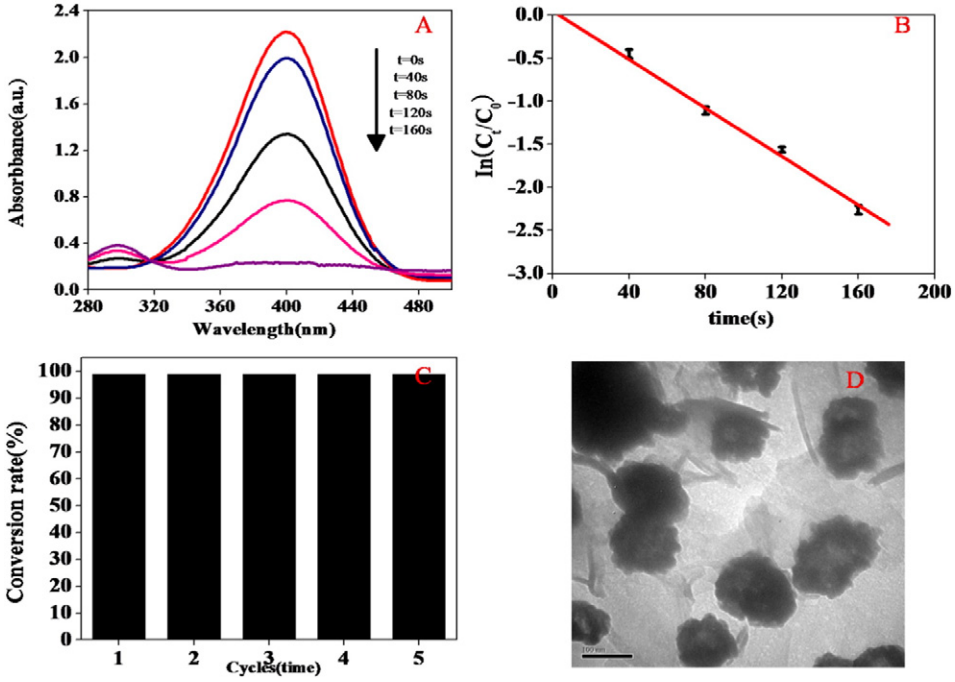

Fig. 6. Time-dependent UV–vis absorption spectra of the 4-nitrophenol reduced by $NaBH_4$ catalyzed by the $Cu/Cu_2O/CuO$ composites(A), plot of $\ln(C_t/C_0)$ versus time for catalyst(B), catalyst recycling efficiency(C), TEM image of catalyst after five cycles(D).

Table 1
Comparison of BET and size among materials.

Entry	Materials	BET($m^2 g^{-1}$)	Size(nm)	Amount of catalyst(mg)	Required time(min)	Reference
1	$Cu/Cu_2O/CuO$ carbon	154.6	100	0.1	3	This article
2	Monodisperse Cu_2O and CuO	–	200	0.15	6	Zhang et al., (2006)
3	Cu_2O powder	6	300–500	0.5	10	Hara et al., (1998)
4	Hollow Cu_2O nanospheres	–	100–200	0.5	7	Luo et al., (2007)
5	Nanosized $CuO-CeO_2$	90	60	0.2	6	Yu et al., (2007)
6	Hollow microspheres CuO/Cu_2O	17.1	500–5000	0.22	7.5	Hu et al., (2013)
7	CuO/Cu_2O hollow polyhedrons	9	10,000	0.2	3.3	Hu et al., (2013)
8	Au–Ag/GO	–	7.5	0.3	0.5	Wu et al., (2013)
9	Au/CuO	–	2.0–3.5(μm)	0.08	17.5	Liang et al., (2013)
10	Ag/CLLC	800	10	10	22	Gao et al., (2012)

aminopyridine (4-AP). In this study, $Cu/Cu_2O/CuO$@C was used as catalytic to reduce 4-NP. An obvious adsorption peak of 4-NP solution appeared at 318 nm which was remarkably red-shifted to 400 nm when was added $NaBH_4$ (Fig.5A). This may be according to the formation of 4-nitrophenolate owing to an increase in solution alkalinity after addition of $NaBH_4$ (Yang et al., 2014).

To exclude adsorption interference due to the catalytic effect, 4-NP was adsorbed by $Cu/Cu_2O/CuO$@C for 24 h in the absence of $NaBH_4$. When this was done, little 4-NP was adsorbed to the catalyst. As shown in Fig 6A, complete reduction of 4-NP occurred in 160 s, which is faster than previously reported rates (Zeng et al., 2013; Chu et al., 2011; Posada et al., 2006; Liu et al., 2013; Yao et al., 2015). We did experiment to investigate the adsorption effect in the absence of $Cu/Cu_2O/CuO$@C, the result showed that UV–vis adsorption spectra of 4-NP didn't change during 10 h with the addition of NaBH4 (Fig. 5B). Change of UV–vis absorbance at 415 nm of 4-NP was monitored during the reaction (Fig. 5A), from 2.2 a.u. to almost zero.

Reduction, mainly stimulated by donor BH^{4-} results in release of electrons. The blank test indicates that in the absence of the catalyst, 4-NP is not photolytically degraded, but after addition of the catalyst the concentration decreased significantly within 3 min. The reaction cannot proceed without $NaBH_4$ or $Cu/Cu_2O/CuO$@C. When a small amount of catalyst was added in the presence of an appropriate amount of $NaBH_4$, the characteristic peak of 4-NP disappeared after 3 min. The greater catalytic activity of the material can be ascribed to their large surface areas compared to other Cu_2O particles (Table 1) due to highly porous supporting materials promoting diffusion of pollutant molecules to the metal catalytic sites. The supporting matrices which reported in other literature possess low surface areas, and the nanoparticles are usually imbedded into the supports, results in the poor accessibility of catalysts towards targets (Markova et al., 2013). Thereby the porous structure may accelerate diffusion of reactants and products, which results in more rapid catalytic degradation of pollutants and leads to greater efficiency of catalysis.

During the reaction, the concentration of $NaBH_4$ is present in excess relative to the amount of 4-NP, so it can be considered to be constant and it's concentration does not affect the rate of reductive degradation of 4-NP. Thus, rate constants for the reduction reaction can be described by use of pseudo-first-order kinetics. The ratio of C_t and C_0 is presented by the absorbance ratio at 415 nm. The slop of the line can be considered

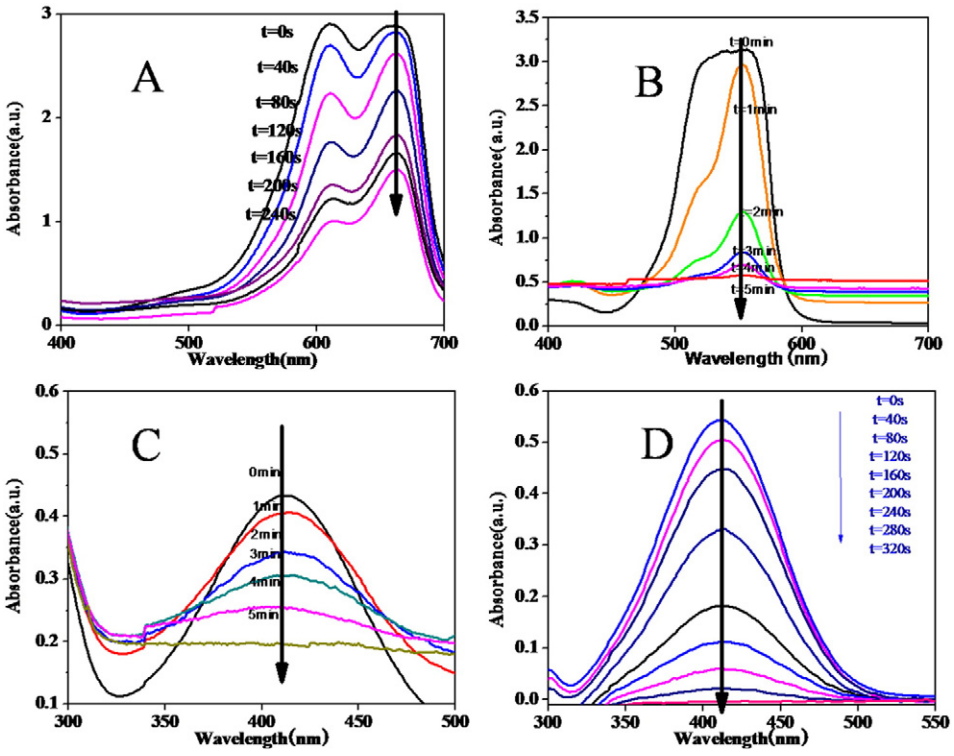

Fig. 7. Time-dependent UV–vis absorption spectra of the MB(A), RhB(B), 2-NP(C), O-NP(D) reduced by $NaBH_4$ catalyzed by the $Cu/Cu_2O/CuO$ composites.

Table 2
Reduction of various pollutants by $Cu/Cu_2O/CuO@C$.

Entry	Compound	Time/min	Conversion
1	*O*-Nitrobenzene methylamine	6	99%
2	Methylene blue	4	56%
3	*O*-Nitrophenol	5	99%
4	Rhodamine B	8	99%

as the reaction rate constant, which in the case of 4-NP was 0.85 min^{-1} (Fig. 6B).

Performance of the catalyst can be assessed by use of an index of stability and reuse. When this was done for catalysis of degradation of 4-NP in water with centrifugal separation of catalyst after each cycle (Fig. 6C) after the 5th cycle reduction of 4-NP was greater than 99%. Thus, stability of the prepared $Cu/Cu_2O/CuO@C$ can be used multiple times with only a moderate decrease in catalytic efficiency. TEM images of reused $Cu/Cu_2O/CuO@C$ showed that the structure and morphology were maintained, which suggested stability of the materials (Fig. 6D).

Catalytic activity of $Cu/Cu_2O/CuO@C$ for other pollutants, including 2-nitrophenol(2-NP), N-nitroaniline(*O*-NP), methylene blue(MB) and rhodamine-B(RhB) (Fig.7) under the same conditions as those used for 4-NP (Table 2). The $Cu/Cu_2O/CuO@C$ exhibited good catalytic activity on degrading a series of nitrobenzene compounds regardless of the types and position of the substituents, and showed excellent yields. The effect of the catalyst on degradation of other $Cu/Cu_2O/CuO@C$ exhibited good catalytic activity with excellent yields toward a series of nitrobenzene compounds regardless of the types and position of the substituents. Three kinds of nitroaniline can be transformed within 8 min with a conversion of 99% and the effect of the substituent position was small. When $Cu/Cu_2O/CuO@C$ was used to catalyze the reduction of nitrotoluene and nitrochlorobenzene, it exhibited lesser activity than for nitroaniline or nitrophenol. One possible reason for this is that reaction processes of nitrotoluene and nitrochlorobenzene are more complicated than those of nitroaniline and nitrophenol (Zeng et al., 2013). For example, the reduction of nitrotoluene and nitrochlorobenzene can produce amino and nitroso form products while nitroaniline and nitrophenol can only be converted into corresponding anilines in the presence of $NaBH_4$ and catalyst (Dotzauer et al., 2009). These results indicate the generality and the efficacy of our new catalyst toward the reduction of different nitrobenzene and we will do more works on the catalytic reaction mechanism of these nitrobenzenes in the future research.

4. Conclusions

In summary, $Cu/Cu_2O/CuO@C$ particles are more efficient and cheaper than noble metal catalyts for degradation of organic pollutants. A simple synthetic route has been developed to fabricate $Cu/Cu_2O/CuO$ particles which adhere to carbon layerers to form a useful catalyst for reductive degradation of pollutants in water. Reaction temperature of 130 °C, molar ratio of 1:1 between gallic acid and $Cu(NO_3)_2 \cdot 6H_2O$ on the morphology and structure are the most appropriate for synthesis. The catalytic effect is comparable to that of noble metal catalysts, but uses less toxic materials. It's outstanding features are: (1) the material combine the advantages metal organic frameworks (MOFs) and Cu-containing materials, the porous structure provided a large contact area and channels for the pollutions and active site. (2) the novel, simple and efficient method to fabricate Cu-MOF by Cu metal and gallic acid (GA). GA has been used in the green synthesis. Reaction temperature of 130 °C, molar ratio of 1:1 between gallic acid and $Cu(NO_3)_2 \cdot 6H_2O$ on the morphology and structure are the most appropriate for synthesis (3). The problem of MOFs weak stability in water has been solved. The carbon support of $Cu/Cu_2O/CuO$ can be used in water. Effective catalysis of reductive degradation of 4-NP indicates the general utility of the catalysis for reductive degradation of similar pollutants.

Acknowledgments

This work was jointly supported by the National Natural Science Foundation of China (41222026, 41521003).

References

Ai, Z.H., Zhang, L.Z., Lee, S.H., Ho, W.K., 2009. Interfacial hydrothermal synthesis of Cu@Cu_2O Core–Shell microspheres with enhanced visible-light-driven photocatalytic activity. J. Phys. Chem. C 113, 20896–20902.
Bai, Y.C., Wu, F.C., Liu, C.Q., Li, W., Guo, J.Y., Fu, P.Q., Xing, B.S., Zheng, J., 2008. Ultraviolet absorbance titration for determining stability constants of humic substances with Cu(II) and Hg(II). Anal. Chim. Acta 616, 115–121.
Bai, Y.C., Lin, D.H., Wu, F.C., Wang, Z.Y., Xing, B.S., 2010. Adsorption of triton X-series surfactants and its role in stabilizing multi-walled carbon nanotube suspensions. Chemosphere 79, 362–367.
Brookshier, M.A., Chusuei, C.C., Goodman, D.W., 1999. Control of CuO particle size on SiO_2 by spin coating. Langmuir 15, 2043–2046.
Chu, S., et al., 2011. Architecture of Cu_2O@TiO_2 core–shell heterojunction and photodegradation for 4-nitrophenol under simulated sunlight irradiation. Mater. Chem. Phys. 129, 1184–1188.
Dhakshinamoorthy, A., Garcia, H., 2012. Catalysis by metal nanoparticles embedded on metal-organic frameworks. Chem. Soc. Rev. 41, 5262–5284.
Dotzauer, D.M., Somnath, B., Wen, Y., et al., 2009. Nanoparticle-containing membranes for the catalytic reduction of nitroaromatic compounds. Langmuir 25, 1865–1871.
Du, T.B., Tamboli, D., Desai, V., 2003. Electrochemical characterization of copper chemical mechanical polishing. Microelectron. Eng. 69, 1–9.
Espinós, J.P., Morales, J., Barranco, A., Caballero, A., Holgado, J.P., González-Elipe, A.R., 2002. Interface effects for Cu, CuO, and Cu_2O deposited on SiO_2 and ZrO_2. XPS determination of the valence state of copper in Cu/SiO_2 and Cu/ZrO_2 catalysts. J. Phys. Chem. B 106, 6921–6929.
Fernando, A N]–>C.A.N., de Silva, H C]–>P.H.C., Wethasinha, S.K., Dharmadasa, I.M., Delsol, T., Simmonds, M.C., 2002. Investigation of n-type Cu_2O layers prepared by a low cost chemical method for use in photo-voltaic thin film solar cells. Renew. Energy 26, 521–529.
Gao, S.Y., Jia, X.X., Li, Z.D., et al., 2012. Hierarchical plasmonic-metal/semiconductor micro/nanostructures: green synthesis and application in catalytic reduction of p-nitrophenol. J. Nanopart Res. 14, 748.
Ghodselahi, T., Vesaghi, M.A., Shafiekhani, A., Baghizadeh, A., Lameii, M., 2008. XPS study of the Cu@Cu_2O core–shell nanoparticles. Appl. Surf. Sci. 255, 2730–2734.
Hara, M., et al., 1998. Cu_2O as a photocatalyst for overall water splitting under visible light irradiation. Chem. Commun. 3, 357–358.
Hu, L., Hong, Y.M., Zhang, F.P., Chen, Q.W., 2013. CuO/Cu_2O composite hollow polyhedrons fabricated from metal–organic framework templates for lithium-ion battery anodes with a long cycling life. Nanoscale 5, 4186–4190.
Hui, W., Xu, J.Z., Zhu, J.J., Chen, H.Y., 2002. Preparation of CuO nanoparticles by microwave irradiation. J. Cryst. Growth 244, 88–94.
Jia, W.Z., Reitz, E., Sun, H., Li, B.K., Zhang, H., Y., L., 2009. From $Cu_2(OH)_3Cl$ to nanostructured sisal-like $Cu(OH)_2$ and CuO: synthesis and characterization. J. Appl. Phys. 105, 064917.
Kreno, L.E., Leong, K., Farha, O.K., Allendorf, M., Van Duyne, R.P., Hupp, J.T., 2012. Metal-organic framework materials as chemical sensors. Chem. Rev. 112, 1105–1125.
Leung, K.C., Xuan, S.H., Zhu, X.M., Wang, D.W., Chak, C.P., Lee, S.F., Ho, W.K., Chung, B.C., 2012. Gold and iron oxide hybrid nanocomposite materials. Chem. Soc. Rev. 41, 1911–1928.
Liang, M., Wang, L.B., Su, R.Q., et al., 2013. Synthesis of silver nanoparticles within cross-linked lysozyme crystals as recyclable catalysts for 4-nitrophenol reduction. Catal. Sci. Technol. 3, 1910–1914.
Liu, J., Wu, Q., Huang, F.L., Zhang, H.F., Xu, S.L., Huang, W., Li, Z.L., 2013. Facile preparation of a variety of bimetallic dendrites with high catalytic activity by two simultaneous replacement reactions. RSC Adv. 3, 14312–14321.
Luo, M.F., Song, Y.P., Lu, J.Q., Wang, X.Y., Pu, Z.Y., 2007. Identification of CuO species in high surface area CuO–CeO_2 catalysts and their catalytic activities for CO oxidation. J. Phys. Chem. C 111, 12686–12692.
Luz, I., Xamena, X L]–>F.X.L., Corma, A., 2010. Bridging homogeneous and heterogeneous catalysis with MOFs: "click" reactions with Cu-MOF catalysts. J. Catal. 276, 134–140.
Markova, Z., Siskova, K.M., Filip, J., et al., 2013. Air stable magnetic bimetallic Fe–Ag nanoparticles for advanced antimicrobial treatment and phosphorus removal. Environ. Sci. Technol. 47, 5285–5293.
Mitchell, L., 2013. Remarkable Lewis acid catalytic performance of the scandium trimesate metal organic framework mil-100(sc) for c–c and cn bond-forming reactions. Catal. Sci. Technol. 3, 606–617.
Niu, H.Y., Liu, S.L., Cai, Y.Q., Wu, F.C., Zhao, X.L., 2016. MOF derived porous carbon supported Cu/Cu_2O composite as high performance non-noble catalyst. Microporous Mesoporous Mater. 219, 48–53.
Panella, B., Hirscher, M., Pütter, H., Müller, U., 2006. Hydrogen adsorption in metal–organic frameworks: cu-MOFs and Zn-MOFs compared. Adv. Funct. Mater. 16, 520–524.
Patricia, H., et al., 2010. Porous metal-organic-framework nanoscale carriers as a potential platform for drug delivery and imaging. Nat. Mater. 9, 172–178.
Posada, D., Betancourt, P., Liendo, F., Brito, J.L., 2006. Catalytic wet air oxidation of aqueous solutions of substituted phenols. Catal. Lett. 106, 81–88.
Schlichte, K., Kratzke, T., Kaskel, S., 2004. Improved synthesis, thermal stability and catalytic properties of the metal-organic framework compound $Cu_3(BTC)_2$. Microporous Mesoporous Mater. 73, 81–88.

SU, D., Yin, P.G., Guo, L., 2011. Synthesis and Raman property of porous jujube-like Cu_2O hierarchy structure. Acta Phys. -Chim. Sin. 27, 1543–1550.
Wagner, C.D., Riggs, W.M., Davis, L.E., Moulder, J.F., Muilenberg, G.E., 1979. Handbook of X-ray Photoelectron Spectroscopy; Perkin-Elmer Corporation Physical Electronics Division: Minnesota.
Wang, W.Z., Zhan, Y.J., Wang, X.S., Liu, Y.K., Zheng, C.L., Wang, G.H., 2002. Synthesis and characterization of CuO nanowhiskers by a novel one-step, solid-state reaction in the presence of a nonionic surfactant. Mater. Res. Bull. 37, 1093–1100.
Wang, W., Liu, Z., Liu, Y., Zheng, C., Wang, G., 2003. A simple wet-chemical synthesis and characterization of CuO nanorods. Appl. Phys. A Mater. Sci. Process. 76, 417–420.
Wu, T., Zhang, L., Gao, J.P., Liu, Y., Gao, C.J., Yan, J., 2013. Fabrication of graphene oxide decorated with Au–Ag alloy nanoparticles and its superior catalytic performance for the reduction of 4-nitrophenol. Mater. Chen. 1, 7384.
Xu, J.F., Li, W., Shen, Z.X., Li, W.S., Tang, H.S., Ye, X.R., Jia, D.Z., Xin, X.Q., 1999. Raman spectra of CuO nanocrystals. J. Raman Spectrosc. 30, 413–415.
Yang, X.L., Zhang, H., Zhu, Y.H., et al., 2014. Highly efficient reusable catalyst based on silicon nanowire arrays decorated with copper nanoparticles. J. Mater. Chem. A 2, 9040–9047.
Yao, W., Li, F.L., Li, H.X., Lang, J.P., 2015. Fabrication of hollow Cu_2O@CuO-supported Au–Pd alloy nanoparticles with high catalytic activity through the galvanic replacement reaction. J. Mater. Chem. A 3, 4578–4585.
Yoosaf, K., Ipe, B.I., Suresh, C.H., Thomas, K.G., 2007. In situ synthesis of metal nanoparticles and selective naked-eye detection of lead ions from aqueous media. J. Phys. Chem. C 111, 12839–12847.
Yu, H.G., Yu, J.G., Liu, S.W., Mann, S., 2007. Template-free hydrothermal synthesis of CuO/Cu_2O composite hollow microspheres. Chem. Mater. 38, 4327–4334.
Zeng, T., Zhang, X.L., Niu, H.Y., Ma, Y.R., Li, W.H., Cai, Y.Q., 2013. In situ growth of gold nanoparticles onto polydopamine-encapsulated magnetic microspheres for catalytic reduction of nitrobenzene. Appl. Catal. B Environ. 134–135, 26–33.
Zhang, J.T., Liu, J.F., Peng, Q., Wang, X., Li, Y.D., 2006. Nearly monodisperse Cu_2O and CuO nanospheres: preparation and applications for sensitive gas sensors. Chem. Mater. 18, 867–871.
Zhao, X.L., Liu, S.L., Tang, Z., Niu, H.Y., Cai, Y.Q., Meng, W., Wu, F.C., Giesy, J.P., 2015. Synthesis of magnetic metal-organic framework (MOF) for efficient removal of organic dyes from water. Sci. Rep. Uk. 5, 11849.
Zhou, L.J., Zou, Y.C., Zhao, J., Wang, P.P., Feng, L.L., Suna, L.W., Wang, D.J., Li, G.D., 2013. Facile synthesis of highly stable and porous Cu_2O/CuO cubes with enhanced gas sensing properties. Sensors Actuators B Chem. 188, 533–539.
Zhu, J.W., Chen, H.Q., Liu, H.B., Yang, X.J., Lu, L.D., Wang, X., 2004. Needle-shaped nanocrystalline CuO prepared by liquid hydrolysis of $Cu(OAc)_2$. Mater. Sci. Eng., A 384, 172–176.
Zhu, M.Y., Wang, C.J., Meng, D.H., Diao, G.W., 2013. In situ synthesis of silver nanostructures on magnetic Fe_3O_4@C core–shell nanocomposites and their application in catalytic reduction reactions. J. Mater. Chem. A 1, 2118–2125.